

Accelerated fMRI reconstruction using Matrix Completion with Sparse Recovery via Split Bregman

Priya Aggarwal^{a,*}, Anubha Gupta^a

^a*SBILab, Department of Electronics and Communication Engineering, Indraprastha Institute of Information Technology (IIIT), Delhi, India*

Abstract

In this work, we propose a new method of accelerated functional MRI reconstruction, namely, Matrix Completion with Sparse Recovery (MCwSR). The proposed method combines low rank condition with transform domain sparsity for fMRI reconstruction and is solved using state-of-the-art Split Bregman algorithm. We compare results with state-of-the-art fMRI reconstruction algorithms. Experimental results demonstrate better performance of MCwSR method compared to the existing methods with reference to normalized mean squared error (NMSE) and other reconstruction quality metrics. In addition, the proposed method is able to preserve voxel activation maps on brain volume. None of the other existing methods is able to demonstrate this property. This shows that the proposed method is accurate and faster, and preserves the voxel activation maps that is the key to study fMRI data.

Keywords: Accelerated functional MRI, nuclear norm, l^1 minimization, sparse recovery, compressed sensing

1. Introduction

Functional magnetic resonance imaging (fMRI) has drawn considerable attention for neuroscience research and clinical applications [1, 2, 3]. fMRI signal, also known as Blood oxygen level dependent (BOLD) signal, is $T2^*$ weighted imaging that consists of 3D brain volumes captured over time [4]. One limitation of fMRI is the long scanning time that leads to annoyance in patients resulting in low signal-to-noise ratio (SNR) due to subject's movement [5]. To this end, compressed sensing (CS) is gaining a lot of interest in recent times for fMRI recovery [6, 7, 8, 9, 10].

*Corresponding author

Email addresses: priyaa@iiitd.ac.in (Priya Aggarwal), anubha@iiitd.ac.in (Anubha Gupta)

Compressive sensing allows reconstruction of fMRI brain volumes using smaller number of k -space measurements that are picked up at sampling rate below the required Nyquist sampling frequency [11]. This reconstruction using lesser samples leads to reduction in scanning time because scanning time is directly related to the number of sampling measurements. Faster scanning implies lower repetition time (TR) and hence, higher sampling frequency. This allows larger bandwidth of signal to be reconstructed without aliasing noise [12]. Thus, not only the quality of reconstructed signal improves, we have more information because of larger signal bandwidth permitted. This further improves the statistical power in BOLD signal that is advantageous in fMRI applications such as disease diagnosis, study of brain functional networks, etc [13]. Thus, reconstruction using lesser samples is extremely advantageous. This is to note that CS based recovery is being extensively used in many other applications such as in other medical imaging modalities [14, 15] and in videos [16, 17].

Conventional fMRI scanners reconstruct fMRI brain volumes (consisting of image slices captured in axial, sagittal, or coronal planes) by applying direct inverse Fourier transform (IFT) to the k -space scanner captured data. However, direct IFT yields noisy reconstruction owing to magnetic deformities, motion artifacts, and movement of gradient coils employed in scanners. To counter these problems, optimization based methods are increasingly been proposed for fMRI reconstruction in recent times. These methods are largely based on compressive sensing strategy.

Compressive sensing based fMRI reconstruction recovers volumes from undersampled k - t space measurements. Compressed sensing solves a set of under-determined equations that has infinitely many solutions. In order to recover a unique solution that corresponds to the recovered signal of interest, regularization terms are added. Many methods have been developed for CS based fMRI reconstruction [6, 7, 8, 9, 10]. These methods can be largely divided into two categories. First category includes online methods that can be implemented as causal systems in real time [6, 7]. These methods implement volume-by-volume reconstruction wherein volume at time t is reconstructed using reconstructed volume of time $t - 1$, hence, assuming causality in the reconstruction framework. Second category includes offline methods that first store k -space data of all fMRI volumes and later, utilize this complete information across both time and space, also called k - t space data, to reconstruct fMRI volumes [8, 9, 10].

In [6, 7], each fMRI slice is reconstructed separately over time. These methods fall in the category of online recursive methods. In both these methods, each slice at time point t is assumed to be the sum of slice at time point $t-1$ and some additional information or residual. While the slice at time point $t-1$ is known, this residual is unknown. In [6], sparsity constraint is imposed on this residual in the CS framework. In [7], mutual information between slice at time t and time $t-1$ is maximized and correspondingly, residual is estimated using linear dynamic sparse modeling.

Methods [8, 9, 10] are offline methods. For example, in [8], fMRI data is reconstructed in CS framework by adding sparsity on the fMRI data in the wavelet domain as a regularization term or constraint. Daubechies wavelet is

used as the sparsifying basis and applied to fMRI brain volumes on a slice-by-slice basis, i.e., every slice of brain volume is captured over all time points and stacked as columns to form a matrix. Reconstruction of each such matrix corresponding to a slice is done separately.

In [9], CS is utilized for fMRI reconstruction by adding rank deficiency as a constraint. It is assumed that the fMRI volume data is low rank having a small number of significant singular values. Accordingly, iterative hard thresholding algorithm is used to recover low-rank observation matrix. However, this method, also called as *k-t FASTER* method, requires rank specification. This method is also called matrix completion owing to signal recovery from low rank observation matrix. In another work [10], fMRI reconstruction is performed using low-rank plus sparse (LR+S) decomposition of the fMRI signal. Here, an iterative framework is used wherein the low rank and sparse components of fMRI data are reconstructed separately.

In this paper, we propose a new fMRI reconstruction method. The salient contribution of this paper are as follows:

1. We apply both matrix completion (MC) and sparse recovery in CS based fMRI reconstruction to improve the reconstruction accuracy. We name the proposed method as Matrix completion with Sparse Recovery (MCwSR). To the best of our knowledge, this method has not been used in fMRI reconstruction so far. Since this proposed method is offline reconstruction method, their performance has been compared with other offline methods such as direct inverse Fourier transform (IFT), CS with wavelet sparsity [8], *k-t FASTER* [9], and LR+S [10].
2. We demonstrate that the proposed MCwSR method is able to preserve voxel activation maps on brain volume, while existing methods provide false activation that may lead to misleading findings on fMRI data. This shows the superior performance of the proposed method in fMRI application and provides a mechanism to test an fMRI reconstruction method beyond NMSE.
3. While the existing *k-t FASTER* method requires rank specification for hard thresholding, we modified this method using soft thresholding and name it *modified k-t FASTER* method. Although it provides improved performance in terms of NMSE (but inferior to the proposed MCwSR method), it is computationally expensive.
4. Interestingly, the performance of fMRI reconstruction in CS setting while imposing sparsity in the Fourier domain (CSFD) is not demonstrated or compared. We observed fMRI data to be sparse in the Fourier domain and checked reconstruction quality with the CSFD method. We observe this method to be performing second best to the proposed MCwSR method that is worth consideration.

This paper is organized into six sections. Section 2 briefly presents compressive sensing based fMRI reconstruction. Section 3 briefly mentions the real

dataset used in this work. Section 4 describes the proposed MCwSR method implemented via Split Bregman iterative algorithm. Experimental results on fMRI data are presented in Section 5. We provide both quantitative and qualitative reconstruction results in section 5 to illustrate the reconstruction quality. In the end, conclusions are presented in section 6.

2. CS based fMRI Reconstruction

A functional MRI data is a 4-dimensional data with 3D brain volume captured over number of time points. This data is represented as belonging to 4D space $\mathbb{R}^{n_x \times n_y \times n_z \times T}$ where n_z is the number of brain slices (or images) along z -axis with each slice of size of $n_x \times n_y$. In slice by slice fMRI reconstruction, Casorati matrix [18] is formed corresponding to all time points of each slice such that the size of the matrix is $n \times T$, where $n = n_x \times n_y$ is the number of voxels in each brain slice and T is the number of brain volumes. Thus, Casorati matrix is formed by stacking one fMRI slice over each time point as one column of the matrix.

Let us consider one such matrix \mathbf{X} corresponding to a single slice captured over T time points. In compressive sensing based reconstruction, undersampled fMRI data is acquired in k -space with a sampling rate that is below the Nyquist rate. The fMRI reconstruction problem from undersampled k -space can be represented as follows:

$$\mathbf{Y} = \Phi \mathbf{F} \mathbf{X} + \xi, \quad (1)$$

where \mathbf{Y} denotes the compressively sensed $k-t$ space data, \mathbf{F} denotes the 2-D Fourier transform operator applied on Casorati matrix \mathbf{X} of one slice, Φ is the sensing matrix that contains partial measurements of $k-t$ space, and $\xi \in \mathbb{R}^{n \times T}$ denotes the measurement noise. The aim of fMRI reconstruction problem is to recover Casorati data matrix \mathbf{X} , given partial Fourier measurements \mathbf{Y} and the sensing matrix Φ . Reconstruction is done independently for all n_z brain slices.

3. Dataset Description

In this paper, we have utilized two publicly available fMRI dataset. These data are available from the openfMRI repository¹.

Dataset-1 [19]: This dataset consists of 36 acquisitions of interleaved brain slices of size 72x72 each at every time point. The data is captured at 179 time points, resulting in a matrix \mathbf{X} of size 5184x179. During the false belief experiment, the subject had to answer questions about stories that referred to either person’s false belief (mental trials) or to outdated physical representations such as an old photograph. For more details on this dataset, please refer to [19].

¹<https://openfmri.org/data-sets>

Dataset-2 [20]: This dataset consists of 33 acquisitions of contiguous brain slices of size 64x64 each at every time point. The data is captured at 300 time points, resulting in a matrix \mathbf{X} of size 4096x300. Subjects were asked to perform the balloon risk-taking task in an event-related design. In this task, there is a chance to earn money by clicking the balloon. Each click increases the size of the balloon that may lead to balloon explosion by over-inflation and hence, the risk. For more details of this data, please refer to [20].

4. Proposed fMRI Reconstruction Method

In this section, we present the proposed MCwSR method that is aimed to provide efficient accelerated fMRI reconstruction using undersampled k -space measurements.

4.1. Proposed MCwSR Method

In this method, we propose to utilize both matrix completion and sparsity in the CS framework for the fMRI reconstruction and hence, name it as Matrix completion with Sparse Recovery (MCwSR) method.

We assume data matrix \mathbf{X} to be low rank [9]. In order to show the validity of this assumption, we plot the sorted singular values of fMRI data matrix \mathbf{X} corresponding to middle slice (slice no. 18) of one subject of dataset-1 in Fig.1. The rapid decay of sorted singular values in Fig.1 indeed confirms the low rank nature of fMRI data.

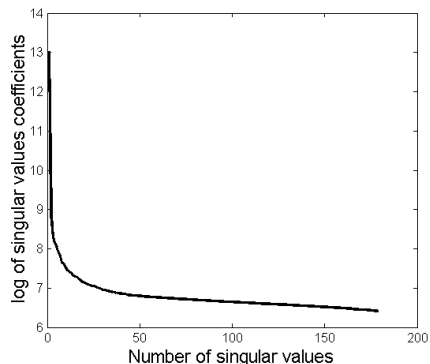
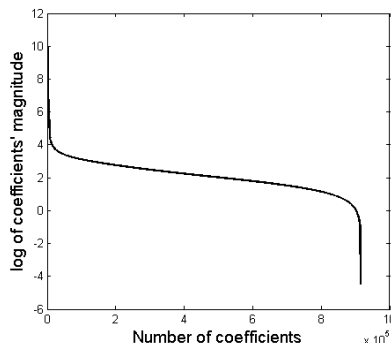
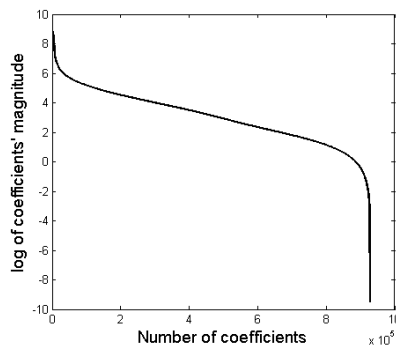


Figure 1: Decay of singular values of fMRI data

In general, sparsity is imposed on the transform domain data. In order to figure out the domain where this fMRI data is more sparse, we plot the sorted transform domain coefficients of matrix \mathbf{X} corresponding to the middle slice (slice no. 18) of one subject of dataset-1 in: a) frequency domain (FD) and b) wavelet domain (Refer to Fig.2). From these figures, we observe that fMRI data is sparser in the frequency domain. Thus, in addition to the assumption of low rank on the observation matrix \mathbf{X} , we assume it to be sparse in the frequency



(a) Sorted magnitude values of Frequency domain coefficients



(b) Sorted coefficients obtained using dB4 wavelet with 3-level decomposition

Figure 2: Sorted magnitude values of coefficients in transform domain

domain. This motivates us to exploit both low-rank and sparsity constraints in fMRI reconstruction which has not been done earlier in the fMRI literature. Thus, we formulate the proposed MCwSR fMRI reconstruction problem as below:

$$\hat{\mathbf{X}} = \arg \min_{\mathbf{X}} \|\mathbf{Y} - \Phi \mathbf{F} \mathbf{X}\|_F^2 + \mu_1 \|\mathbf{X}\|_* + \mu_2 \|\Psi \mathbf{X}\|_1, \quad (2)$$

where $\| \cdot \|_F$ denotes the Frobenius norm which is defined as $\|\mathbf{Y} - \Phi \mathbf{F} \mathbf{X}\|_F^2 = \text{Tr}[(\mathbf{Y} - \Phi \mathbf{F} \mathbf{X})^T (\mathbf{Y} - \Phi \mathbf{F} \mathbf{X})]$. $\|\cdot\|_1$ denotes l^1 norm, defined as absolute sum of entries in a matrix. $\|\cdot\|_*$ denotes the nuclear norm which is the l^1 norm of its singular values. Ψ denotes the Fourier transform in the temporal direction. μ_1 and μ_2 are the regularization parameters.

The two regularization terms in (2) imply low rank and sparsity constraints on Casorati observation matrix \mathbf{X} , respectively. First regularization term associated with μ_1 in the above model assumes matrix \mathbf{X} to be low rank. Second regularization term in the above model assumes $\Psi \mathbf{X}$ to be sparse in the Fourier domain (FD). Both these regularization terms are non-smooth and involve \mathbf{X} . There is no off-the-shelf algorithm to solve (2) and hence, we utilize Split Bregman algorithm [21, 22] that splits this problem into multiple subproblems that

are easier to solve. Next, we explain Split Bregman based methodology to solve this problem.

4.1.1. Low Rank and Sparse CS Recovery via Split Bregman

This methodology is based on Bregman type variable splitting with alternating direction method of multipliers (ADMM) [23]. It utilities variable splitting to decompose original problem into easier subproblems. We introduce two proxy variables \mathbf{Z} and \mathbf{W} for the last two regularization terms in (2) [23]. It allows solving (2) via splitting it into subproblems. The new objective function is:

$$\begin{aligned} \hat{\mathbf{X}} = \arg \min_{\mathbf{X}, \mathbf{Z}, \mathbf{W}} & \|\mathbf{Y} - \Phi \mathbf{F} \mathbf{X}\|_F^2 + \mu_1 \|\mathbf{W}\|_* + \mu_2 \|\Psi \mathbf{Z}\|_1 + \\ & \text{s.t. } \mathbf{W} = \mathbf{X} \text{ and } \mathbf{Z} = \mathbf{X}. \end{aligned} \quad (3)$$

Here, \mathbf{W} and \mathbf{Z} are acting as a proxy for variable of interest \mathbf{X} . Following [23], we substitute equality constraints for each of the proxy variables to split (3) and introduce Bregman variables, also known as augmented Lagrangian multipliers, \mathbf{B}_1 and \mathbf{B}_2 to solve (3) as below:

$$\begin{aligned} \hat{\mathbf{X}} = \arg \min_{\mathbf{X}, \mathbf{Z}, \mathbf{W}} & \|\mathbf{Y} - \Phi \mathbf{F} \mathbf{X}\|_F^2 + \mu_1 \|\mathbf{W}\|_* + \mu_2 \|\Psi \mathbf{Z}\|_1 + \\ & \frac{\eta_1}{2} \|\mathbf{W} - \mathbf{X} - \mathbf{B}_1\|_F^2 + \frac{\eta_2}{2} \|\mathbf{Z} - \mathbf{X} - \mathbf{B}_2\|_F^2, \end{aligned} \quad (4)$$

where η_1 and η_2 are regularization parameters and, \mathbf{B}_1 and \mathbf{B}_2 are the Bregman variables used to enforce equality between original and proxy variables. The above equation consists of three variables \mathbf{W} , \mathbf{Z} , and \mathbf{X} along with two more variables, \mathbf{B}_1 and \mathbf{B}_2 . We split the above problem into three subproblems. Each subproblem may be treated as minimization over one variable while fixing other variables. We use an alternating minimizing scheme to solve (4) which alternatively updates each three variables along with Bregman variables updates until convergence. The pseudo code of the algorithm is provided in Algorithm-1.

This is an iterative method for iterations $j=1, 2, \dots$. Each iteration comprises of four steps: a) Update of proxy variable \mathbf{W}^j ; b) Update of proxy variable \mathbf{Z}^j ; c) Update of \mathbf{X}^j d) Update of Bregman variables \mathbf{B}_1^j and \mathbf{B}_2^j , where j is an iteration number. We stop iterations either by comparing objective function value in (2) with predefined tolerance value or stopping with fixed number of iterations.

The solution of each subproblem is explained in the following subsections.

4.1.2. \mathbf{W} -subproblem

The first subproblem is nuclear norm minimization of matrix \mathbf{W} as shown in Algorithm-1. We solve this subproblem using soft thresholding [24]. Soft thresholding is found to be one of the best method among the many existing algorithms [24, 25] for low rank matrix recovery. The solution of \mathbf{W} -subproblem

is summarized in Algorithm-2.

Algorithm 1 Pseudo code of proposed MCwSR method

- 1: Intialize $\mu_1, \mu_2, \eta_1, \eta_2, \mathbf{B}_1^0, \mathbf{B}_2^0, \mathbf{X}^0, j=1$
- 2: **while** convergence criteria not met **do**
- 3: **W**-subproblem

$$\mathbf{W}^j = \arg \min_{\mathbf{W}} \mu_1 \|\mathbf{W}\|_* + \frac{\eta_1}{2} \left\| \mathbf{W} - \mathbf{X}^{j-1} - \mathbf{B}_1^{j-1} \right\|_F^2.$$

- 4: **Z**-subproblem

$$\mathbf{Z}^j = \arg \min_{\mathbf{Z}} \mu_2 \|\Psi \mathbf{Z}\|_1 + \frac{\eta_2}{2} \left\| \mathbf{Z} - \mathbf{X}^{j-1} - \mathbf{B}_2^{j-1} \right\|_F^2$$

- 5: **X**-subproblem

$$\mathbf{X}^j = \arg \min_{\mathbf{X}} \|\mathbf{Y} - \Phi \mathbf{F} \mathbf{X}\|_F^2 + \frac{\eta_1}{2} \left\| \mathbf{W}^j - \mathbf{X} - \mathbf{B}_1^{j-1} \right\|_F^2 + \frac{\eta_2}{2} \left\| \mathbf{Z}^j - \mathbf{X} - \mathbf{B}_2^{j-1} \right\|_F^2.$$

- 6: **Bregman variable update**

$$\begin{aligned} \mathbf{B}_1^j &= \mathbf{B}_1^{j-1} + \mathbf{X}^j - \mathbf{W}^j. \\ \mathbf{B}_2^j &= \mathbf{B}_2^{j-1} + \mathbf{X}^j - \mathbf{Z}^j. \end{aligned}$$

- 7: $j=j+1$
 - 8: **end while**
-

SVD of the matrix \mathbf{W}^j is required to be computed as in step 2 of Algorithm 2. Since direct SVD computation is time intensive due to large size of the observation matrix, a different strategy is adopted to minimize computational complexity. Instead of direct SVD computation, singular values and right singular vectors are determined using eigen decomposition of $(\mathbf{W}^j)^H \mathbf{W}^j$ as below:

$$(\mathbf{W}^j)^H \mathbf{W}^j = \mathbf{V} \mathbf{S}^2 \mathbf{V}^T, \quad (5)$$

where H denotes matrix Hermitian transpose. Left singular vectors \mathbf{U} are determined from $\mathbf{W}^j = \mathbf{U} \mathbf{S} \mathbf{V}^T$ where \mathbf{W}^j , singular values matrix \mathbf{S} , and the right singular vectors' matrix \mathbf{V} are known. This completes the SVD computation of matrix \mathbf{W}^j .

4.1.3. **Z**-subproblem

The second subproblem is analysis prior l^1 minimization problem. For any analysis prior l^1 minimization problem such as

$$\min_{\mathbf{P}} \alpha \|\Psi \mathbf{P}\|_1 + \frac{\beta}{2} \|\mathbf{P} - \mathbf{Q}\|_F^2, \quad (6)$$

Algorithm 2 Pseudo code of \mathbf{W} -subproblem in Algorithm-1

- 1: Initialize $\mathbf{W}^j = \mathbf{X}^{j-1} + \mathbf{B}_1^{j-1}$.
- 2: Compute singular value decomposition (SVD) of $\mathbf{W}^j = \mathbf{U}\mathbf{S}\mathbf{V}^T$, where \mathbf{U} and \mathbf{V} are the matrices containing left and right singular vectors, respectively, and the matrix \mathbf{S} contains the singular values.
- 3: Soft thresholding is applied on the singular values contained on diagonal of \mathbf{S} as

$$\mathbf{\Gamma} = \text{Soft}(\mathbf{S}, \frac{\mu_1}{\eta_1} \mathbf{I}) = \text{sgn}(\mathbf{S}) \otimes \max \left\{ 0, |\mathbf{S}| - \frac{\mu_1}{\eta_1} \mathbf{I} \right\},$$

where \otimes denotes the element-wise product, $|\mathbf{S}|$ denotes absolute values of matrix \mathbf{S} and \mathbf{I} is identity matrix. \mathbf{I} in the above equation ensures soft thresholding only on diagonal elements of \mathbf{S} . For the nonzero elements of \mathbf{S} , $\text{sgn}(\mathbf{S}) = \mathbf{S} / |\mathbf{S}|$, otherwise $\text{sgn}(\mathbf{S}) = 0$.

- 4: Next, \mathbf{W}^j is updated with updated singular values and older singular matrices

$$\mathbf{W}^j = \mathbf{U}\mathbf{\Gamma}\mathbf{V}^T,$$

where $\mathbf{P}, \mathbf{Q} \in \mathbf{R}^{n \times T}$ and $\alpha, \beta > 0$, the solution is [26]

$$\mathbf{P} = \mathbf{\Psi}^H(\text{Soft}(\mathbf{\Psi}\mathbf{Q}, \frac{\alpha}{\beta} \mathbf{A})), \quad (7)$$

where \mathbf{A} is a matrix containing all ones, \mathbf{Q} is the initial estimate of \mathbf{P} , and 'Soft' is defined as

$$\text{Soft}(\mathbf{\Psi}\mathbf{Q}, \frac{\alpha}{\beta} \mathbf{A}) = \text{sgn}(\mathbf{\Psi}\mathbf{Q}) \otimes \max \left\{ 0, |\mathbf{\Psi}\mathbf{Q}| - \frac{\alpha}{\beta} \mathbf{A} \right\}, \quad (8)$$

where \otimes denotes the element-wise product, $|\mathbf{\Psi}\mathbf{Q}|$ denotes absolute values of matrix $\mathbf{\Psi}\mathbf{Q}$. For the nonzero elements of $\mathbf{\Psi}\mathbf{Q}$, $\text{sgn}(\mathbf{\Psi}\mathbf{Q}) = \mathbf{\Psi}\mathbf{Q} / |\mathbf{\Psi}\mathbf{Q}|$, otherwise $\text{sgn}(\mathbf{\Psi}\mathbf{Q}) = 0$.

Hence, the closed form solution of \mathbf{Z} at iteration j in \mathbf{Z} -subproblem is

$$\mathbf{Z}^j = \mathbf{\Psi}^H(\text{Soft}(\mathbf{\Psi}(\mathbf{X}^{j-1} + \mathbf{B}_2^{j-1}), \frac{\mu_2}{\eta_2} \mathbf{A})), \quad (9)$$

where $\mathbf{\Psi}^H$ denotes the Hermitian transpose of the sparsifying basis $\mathbf{\Psi}$ used in (9).

4.1.4. \mathbf{X} -subproblem

With fixed \mathbf{W} and \mathbf{Z} , this subproblem is quadratic as shown in Algorithm-1. It can be solved using conjugate gradient algorithm [27]. Last step in Algorithm-1 is the update of Bregman variables that is explained in Algorithm-1.

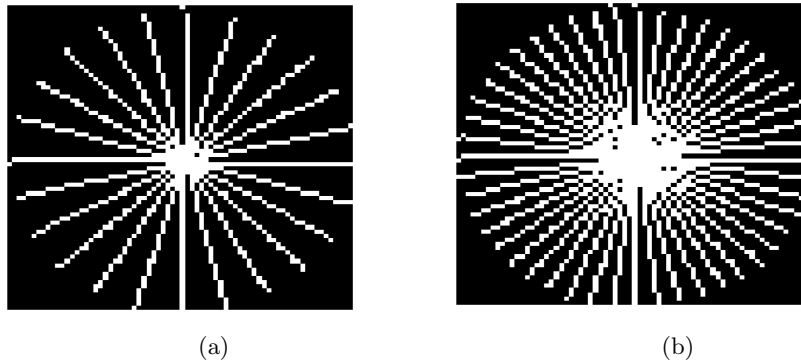


Figure 3: Radial sampling pattern of one slice: (a) 12 radial lines (6.065 acceleration factor); (b) 24 radial lines (3.495 acceleration factor)

5. Experimental Results

In this section, we present results of the proposed MCwSR method in fMRI reconstruction and compare these results with some of the existing state-of-the-art algorithms.

5.1. Sampling of k -space Data

Since the raw k - t space data is not available from the above dataset, we simulated the undersampled measurement data \mathbf{Y} required for testing the proposed methods by computing the Fourier transform of \mathbf{X} followed by undersampling using Φ as described in [28]. This is a standard methodology in any reconstruction related research work. Fig.3 shows two different radial sampling measurement patterns. As evident from Fig.3, these radial measurement patterns sample more data points in the low frequency region compared to the high frequency region.

We consider different sampling patterns for each time point data in order to maintain incoherency amongst the columns of matrix \mathbf{X} [28]. Radial sampling is chosen because this is by far the fastest k -space sampling method in real time application [28]. Please note that our work is general and can be used with any sampling pattern.

5.2. Brief Description of Methods Implemented

We compare results of the proposed MCwSR method with other offline fMRI reconstruction methods including CS with wavelet sparsity [8], k - t FASTER [9], LR+S [10], etc. In addition, we have implemented proposed *modified k-t FASTER* and CSFD methods. Below we present brief overview of each reconstruction method implemented. We also provide parameter values used in the simulation of these methods.

5.2.1. *k-t FASTER method [9]*

k-t FASTER method reconstructs fMRI data assuming data matrix \mathbf{X} to be low rank. This method is implemented by solving the below optimization problem [9]:

$$\hat{\mathbf{X}} = \arg \min_{\mathbf{X}} \|\mathbf{Y} - \Phi \mathbf{F} \mathbf{X}\|_F^2 \quad s.t \quad rank(\mathbf{X}) = r, \quad (10)$$

where r is pre-defined rank of \mathbf{X} . In *k-t FASTER* [9], hard thresholding is applied on the singular values of data matrix \mathbf{X} as explained below. First, SVD of an initial crude estimate of matrix \mathbf{X} is computed

$$\mathbf{X} = \mathbf{U} \mathbf{S} \mathbf{V}^T. \quad (11)$$

Next, hard thresholding is applied on the singular values contained in \mathbf{S} as

$$\hat{s}_i = \begin{cases} |s_i| - \mu & i \leq r \\ 0 & i > r \end{cases} \quad (12)$$

where μ is a constant, s_i is i^{th} singular value of \mathbf{S} , and \hat{s}_i is updated singular value after hard thresholding.

The value of constant μ is chosen to be 0.5 as used in [9]. In the simulation, rank r is taken to be equal to the number of time frames. This value provided least normalized mean square error (NMSE) between reconstructed and original fMRI data on the two dataset considered in this work.

5.2.2. *Proposed Modified k-t FASTER*

Pre-defined rank of \mathbf{X} with hard thresholding on its singular values is imposed in *k-t FASTER* method explained above for fMRI reconstruction. Pre-defined hard-thresholding of rank may not provide best results as significant information may be contained in data associated with the rejected/dropped singular values. Thus, we propose to solve fMRI low rank reconstruction problem by soft thresholding [24]. To the best of our knowledge this method so far has not been used in fMRI for reconstruction. We name this method as proposed modified *k-t FASTER*.

In this method, the reconstruction problem is formulated as below:

$$\hat{\mathbf{X}} = \arg \min_{\mathbf{X}} \|\mathbf{Y} - \Phi \mathbf{F} \mathbf{X}\|_F^2 + \lambda_1 \|\mathbf{X}\|_*, \quad (13)$$

where λ_1 is regularization parameter and $\|*\|$ is the nuclear norm. This problem is solved iteratively using soft thresholding equation as used in Algorithm-2.

This proposed method does not require pre-defined rank specification and hard thresholding on the singular values unlike *k-t FASTER* method which is not a practical solution. Rather, this proposed modification is general enough to exploit rank deficiency in matrix completion.

We compared normalized mean square error (NMSE) results on signal reconstruction for different values of λ_1 ranging between 10 to 500. We obtained minimum NMSE with $\lambda_1 = 300$. Hence, we empirically selected $\lambda_1 = 300$ in (13).

5.2.3. Low rank plus sparse (LR+S) method [10]

This method reconstructs fMRI data using low rank and sparse matrix decomposition and hence, is solved using the following optimization framework:

$$\hat{\mathbf{L}}, \hat{\mathbf{S}} = \arg \min_{\mathbf{L}, \mathbf{S}} \|\mathbf{Y} - \Phi \mathbf{F}(\mathbf{L} + \mathbf{S})\|_F^2 + \lambda_2 \|\mathbf{L}\|_* + \lambda_3 \|\mathbf{S}\|_1, \quad (14)$$

where λ_2 and λ_3 are regularization parameters. The fMRI data matrix \mathbf{X} is reconstructed as:

$$\hat{\mathbf{X}} = \hat{\mathbf{L}} + \hat{\mathbf{S}}. \quad (15)$$

We empirically selected $\lambda_2 = 200$ and $\lambda_3 = 2$ in (14) that provided us minimum NMSE.

5.2.4. CS with wavelet sparsity (CSWD) [8]

In this method, compressive sensing based reconstruction of fMRI data is carried out assuming the fMRI data to be sparse in the wavelet domain [8]. Hence, fMRI reconstruction is done by using the below optimization framework:

$$\hat{\mathbf{X}} = \arg \min_{\mathbf{X}} \|\mathbf{Y} - \Phi \mathbf{F} \mathbf{X}\|_F^2 + \lambda_4 \|\mathbf{W} \mathbf{X}\|_1, \quad (16)$$

where λ_4 is regularization parameter and \mathbf{W} is a wavelet matrix operator. We used Daubechies' orthogonal wavelet 'db4' (filter lengths 8) with 3-level decomposition as has been used in [8].

5.2.5. CS with frequency domain sparsity (CSFD)

It has been shown in Fig.2 above that the fMRI data is sparser in the frequency domain compared to the wavelet domain. Thus, we propose to test fMRI reconstruction using compressive sensing with Fourier domain (FD) sparsity. We formulate the reconstruction problem as:

$$\hat{\mathbf{X}} = \arg \min_{\mathbf{X}} \|\mathbf{Y} - \Phi \mathbf{F} \mathbf{X}\|_F^2 + \lambda_4 \|\mathbf{F} \mathbf{X}\|_1, \quad (17)$$

where \mathbf{F} is the Fourier matrix operator.

5.2.6. CS with time domain Sparsity (CSTD)

This method of signal reconstruction is also called basis pursuit method [29] and is one of the popular methods of signal reconstruction assuming signal to be sparse in the time domain. Since we implemented CSFD and CSWD, we are also interested in looking at results wherein sparsity is imposed in the time domain (CSTD). Using CSTD, the problem of fMRI reconstruction can be formulated as below:

$$\hat{\mathbf{X}} = \arg \min_{\mathbf{X}} \|\mathbf{Y} - \Phi \mathbf{F} \mathbf{X}\|_F^2 + \lambda_4 \|\mathbf{X}\|_1. \quad (18)$$

All the above three methods CSWD, CSFD, and CSTD require only one parameter λ_4 to be specified in equations (16)-(18). In [30], it is suggested to consider

$$\lambda_4 < \max(\Phi^T(IFT(\mathbf{Y}))). \quad (19)$$

where IFT stands for Inverse Fourier Transform. In order to meet the above condition, we chose

$$\lambda_4 = 0.009 * \max(\Phi^T(IFT(\mathbf{Y}))) \quad (20)$$

that meets (19).

5.2.7. Proposed MCwSR method

The proposed MCwSR method reconstructs using both MC and Sparse Recovery in Fourier domain as formulated in (2) and implemented via (4). This method requires six parameters μ_1 , μ_2 , η_1 , η_2 , \mathbf{B}_1 , and \mathbf{B}_2 to be initialized. Split Bregman algorithm's internal variables are set to $\eta_1=\eta_2=10^{-2}$. Bregman variables \mathbf{B}_1 and \mathbf{B}_2 are initialized to matrices containing all one's. We use *L*-curve method to initialize μ_1 and μ_2 [31]. With this method, we arrive at the following values: $\mu_1=10^2$ and $\mu_2=10^2$. The fMRI data matrix \mathbf{X} in Alogrithm 1 is initialized using crude initial estimate via direct inverse Fourier transform (IFT). Direct IFT method computes IFT of given $k-t$ space data \mathbf{Y} to reconstruct \mathbf{X} as shown below:

$$\hat{\mathbf{X}} = IFT(\mathbf{Y}). \quad (21)$$

5.3. Results

For all of the methods explained above, we set the maximum number of iterations (required in optimization) to be equal to 500. Fig.4 represents the optimization function value versus number of iterations for MCwSR method corresponding to middle slice reconstruction of one subject of dataset-1. In general, maximum no. of iterations should be chosen for any algorithm such that it converges similar to Fig.4. We set the following convergence criteria for all methods: $\text{optimization function value}(\text{end}) - \text{optimization function value}(\text{end} - 1) < 10^{-5}$. All simulation was run on a computer with an Intel Core i7 CPU at 2.4 GHz, and 16 GB of RAM utilizing MATLAB (R2014a: The Mathworks, Natick, MA, USA).

We present reconstruction results, for varying number of radial sampling lines, in terms of normalized mean square error $NMSE = \left\| \mathbf{X} - \hat{\mathbf{X}} \right\|_2 / \left\| \mathbf{X} \right\|_2$, and peak signal-to-noise ratio (PSNR). Table 1 presents reconstruction results on one slice (averaged over all time points). We considered middle slice of both the dataset, slice no. 18 (total slices=36) of dataset-1 and slice no. 16 (total slices=33) of dataset-2. Fig.5 and Fig.6 present corresponding visual results for both the dataset using all methods. We present these results on subject 1 of both dataset.

From figures 5 and 6, we observe that the reconstruction quality with the proposed accelerated modified $k-t$ FASTER and MCwSR method is superior compared to the existing state-of-the-art methods. Interestingly, results with CSFD have not been presented earlier in fMRI reconstruction, although it really

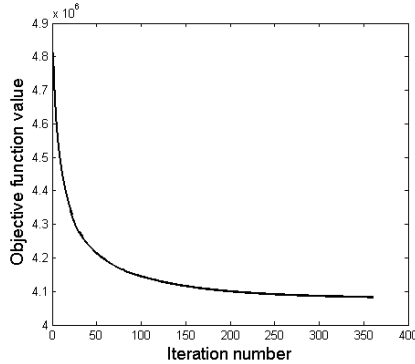


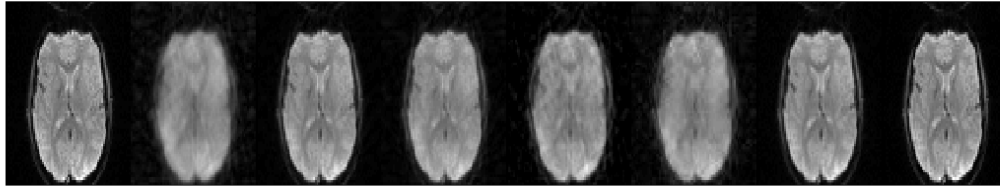
Figure 4: Objective function value versus number of iterations

Table 1: Reconstruction results on a fixed slice (stacked for all time points as Casorati Matrix)

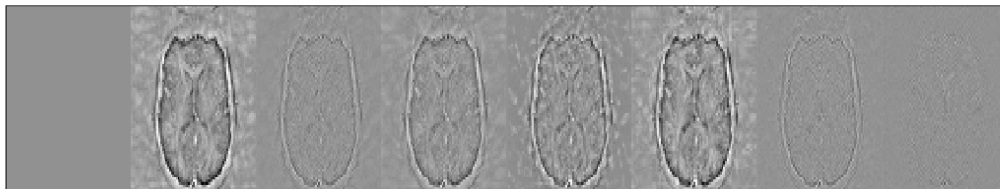
fMRI dataset	Technique	NMSE		PSNR		Computational time	
		12 lines	24 lines	12 lines	24 lines	12 lines	24 lines
Dataset 1	<i>k-t</i> FASTER [9]	0.2359	0.1584	7.29	10.75	12.59	11.65
(Middle slice	Proposed Modified <i>k-t</i> FASTER	0.0764	0.0516	16.68	20.36	267.31	254.48
Slice no.18)	LR+S [10]	0.1374	0.0796	11.95	16.89	55.70	56.72
Subject 1	CSTD (BPDN)	0.1755	0.1099	9.94	13.87	14.61	15.36
No. of time	CSWD [8]	0.2190	0.1380	7.79	12.07	26.09	23.48
Points=179	CSFD	0.0864	0.0579	16.32	19.66	27.9	26.20
	Proposed MCwSR	0.0496	0.0458	20.90	21.55	48.30	47.20
Dataset 2	<i>k-t</i> FASTER [9]	0.1636	0.1098	11.71	15.16	21.52	20.05
(Middle slice	Proposed Modified <i>k-t</i> FASTER	0.0374	0.0355	24.56	24.97	374.29	352.03
Slice no.16)	LR+S [10]	0.1123	0.0360	14.78	25.00	123.42	112.74
Subject 1	CSTD (BPDN)	0.1186	0.0729	14.39	18.88	30.92	28.57
No. of time	CSWD [8]	0.1599	0.1020	12.15	16.12	50.20	51.63
Points=300	CSFD	0.0512	0.0399	21.93	24.28	54.33	53.76
	Proposed MCwSR	0.0406	0.0376	23.65	24.37	90.09	88.17

performs very well. This validates our assumption that the data is indeed sparser in the frequency domain compared to the time domain or the wavelet domain and hence, the choice in the proposed MCwSR method.

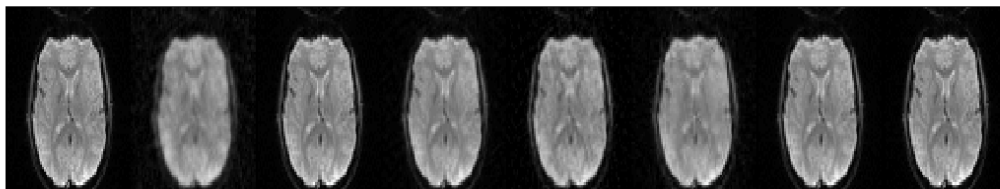
From Table-1, we note that on a single slice reconstruction, modified *k-t* FASTER method seems to be performing better on dataset-2 with reference to the proposed MCwSR method. This is due to fact that dataset-2 has 300 number of time points and dataset-1 has 179 time points. With more number of time points, the rank of matrix \mathbf{X} may reduce on some slices in dataset-2, improving the performance of modified *k-t* FASTER in dataset-2. However, MCwSR method still performs better in terms of computational time on both the dataset. We will see later that, on the entire fMRI volumes and brain slices,



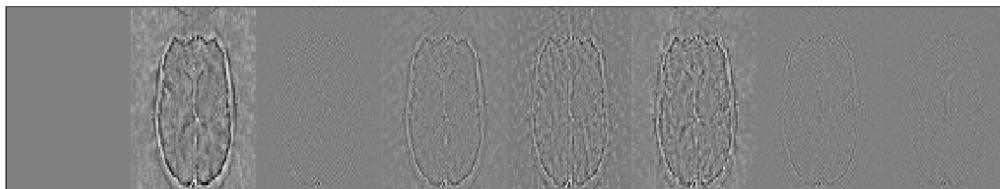
(a) Original and reconstructed slice no. 18, time point 100, 12 radial lines
 left to right: Original; $k-t$ FASTER; Modified $k-t$ FASTER; LR+S; CSTD; CSWD;
 CSFD; Proposed MCwSR



(b) Difference Images (Ground truth - Reconstructed), slice no. 18, time point 100,
 12 radial lines
 left to right: Original; $k-t$ FASTER; Modified $k-t$ FASTER; LR+S; CSTD; CSWD;
 CSFD; Proposed MCwSR

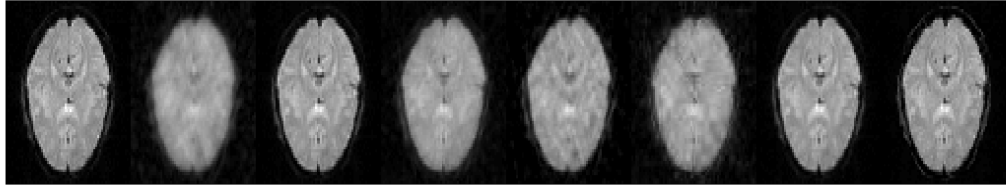


(c) Original and reconstructed slice no. 18, time point 100, 24 radial lines
 left to right: Original; $k-t$ FASTER; Modified $k-t$ FASTER; LR+S; CSTD; CSWD;
 CSFD; Proposed MCwSR

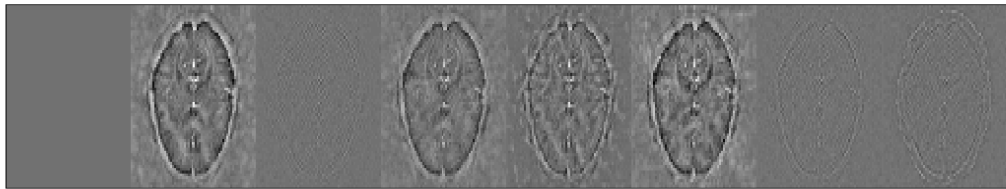


(d) Difference Images (Ground truth - Reconstructed), slice no. 18, time point 100,
 24 radial lines
 left to right: Original; $k-t$ FASTER; Modified $k-t$ FASTER; LR+S; CSTD; CSWD;
 CSFD; Proposed MCwSR

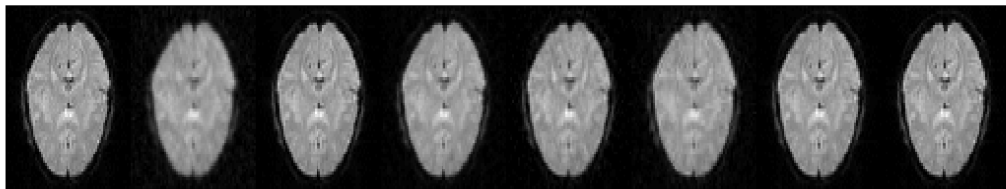
Figure 5: Reconstruction Results on subject 1 Dataset-1: False belief fMRI data



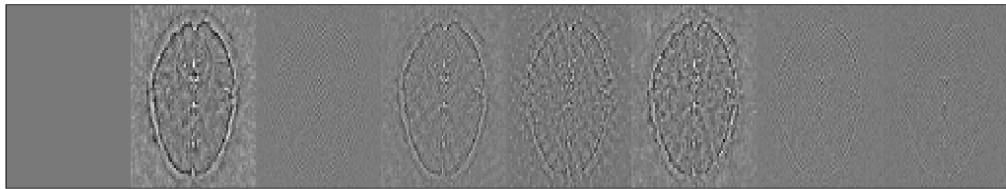
(a) Original and reconstructed slice no. 16, time point 150, 12 radial lines
 left to right: Original; $k-t$ FASTER; Modified $k-t$ FASTER; LR+S; CSTD; CSWD;
 CSFD; Proposed MCwSR



(b) Difference Images (Ground truth - Reconstructed), slice no. 16, time point 150,
 12 radial lines
 left to right: Original; $k-t$ FASTER; Modified $k-t$ FASTER; LR+S; CSTD; CSWD;
 CSFD; Proposed MCwSR



(c) Original and reconstructed slice no. 16, time point 150, 24 radial lines
 left to right: Original; $k-t$ FASTER; Modified $k-t$ FASTER; LR+S; CSTD; CSWD;
 CSFD; Proposed MCwSR



(d) Difference Images (Ground truth - Reconstructed), slice no. 16, time point 150,
 24 radial lines
 left to right: Original; $k-t$ FASTER; Modified $k-t$ FASTER; LR+S; CSTD; CSWD;
 CSFD; Proposed MCwSR

Figure 6: Reconstruction Results on on subject 1 Dataset-2: Balloon risk-taking task
 fMRI data

MCwSR excels in performance in terms of NMSE compared to all the methods implemented.

Computational time analysis

Table 1 shows the computational time of reconstruction of middle slice of subject 1 of both dataset. We observe that computational time is least with CSTD because time domain sparsity does not involve bigger matrix multiplications compared to CSWD and CSFD. On the other hand, modified k - t FASTER is computationally most expensive compared to all methods. This is owing to the fact that this method computes SVD in every iteration that is computationally expensive. Moreover, this method consumes larger number of iterations for convergence. CSFD consumes less time than the proposed MCwSR, however, it observes 2-5 dB PSNR performance loss in dataset-1 and 0-2 dB PSNR performance loss in dataset-2 compared to the MCwSR method. This implies a trade-off between computational time and reconstruction efficiency with reference to MCwSR and CSFD. Please note that in offline reconstruction methods, a little higher computational time in reconstruction can always be compromised provided the reconstruction quality is better and that indeed is the case with the proposed MCwSR method.

Multi slice reconstruction results analysis

Table 2 presents reconstruction results averaged over all volumes and over all slices. Results are tabulated at 6, 12 and 24 number of radial sampling lines. From these results, we observe that the proposed MCwSR consistently performs better in terms of NMSE than the existing reconstruction methods. Computational time in all the methods is roughly equal to the no. of slices x computational time of one slice reconstruction. Since these values were presented in Table 1, hence, the computational time is not repeated for spacious presentation of NMSE results in Table 2.

From Table 2, we observe that NMSE increases for all methods when number of radial lines are reduced (fewer k -space measurements). CS with FD sparsity (CSFD) shows reconstruction performance that is quite close to the modified k - t FASTER. This is to note that the proposed MCwSR method assumes both low-rank (salient feature of modified k - t FASTER) and sparsity in the frequency domain (salient feature of CSFD). Hence, it yields better results compared to all the methods and reconstructs fMRI data quite efficiently at lower number of radial sampling lines.

We also evaluated the performance of all reconstruction methods in terms of signal-to-error ratio (SER) in dB which is defined as

$$SER = -10\log_{10}NMSE. \quad (22)$$

Fig.7a shows the SER vs number of radial lines for middle slice (slice no. 18) of subject 1 of dataset-1. SER curves show that MCwSR outperforms the other reconstruction methods. Also, we observe that SER in case of MCwSR method is consistently very high at all radial sampling lines considered. This implies

Table 2: Averaged NMSE results on all slices of all volume

Dataset	Technique	NMSE			PSNR		
		6 lines	12 lines	24 lines	6 lines	12 lines	24 lines
Dataset 1	$k-t$ FASTER [9]	0.2776	0.2419	0.1633	6.458	8.93	12.37
Subject 1	Proposed Modified $k-t$ FASTER	0.1541	0.0729	0.0510	12.836	19.35	22.76
	LR+S [10]	0.2115	0.1175	0.0680	10.07	15.09	19.99
	CSTD (BPDN)	0.2295	0.1655	0.1042	9.434	12.35	16.38
	CSWD [8]	0.2936	0.2114	0.1187	7.201	10.08	15.11
	CSFD	0.0828	0.0713	0.0542	18.68	19.85	22.16
	Proposed MCwSR	0.0554	0.0519	0.0443	22.27	22.86	23.15
Dataset 2	$k-t$ FASTER [9]	0.3244	0.2171	0.1516	9.856	14.01	17.55
Subject 1	Proposed Modified $k-t$ FASTER	0.1016	0.0835	0.0648	19.91	22.78	26.01
	LR+S [10]	0.2061	0.1282	0.0805	14.83	19.08	23.39
	CSTD (BPDN)	0.2008	0.1490	0.0951	14.71	17.80	21.83
	CSWD [8]	0.2675	0.1974	0.1178	12.21	15.14	19.80
	CSFD	0.0823	0.0703	0.0623	23.08	25.59	26.19
	Proposed MCwSR	0.0713	0.0691	0.0601	25.35	25.70	26.38

that we can reconstruct fMRI data by sampling much lesser measurements in $k-t$ space with the proposed MCwSR method compared to other methods. Hence, higher acceleration is possible with MCwSR method that in turn will decrease the fMRI acquisition time. Fig.7b shows the SER vs number of radial lines for middle slice (slice no. 16) of subject 1 of dataset-2.

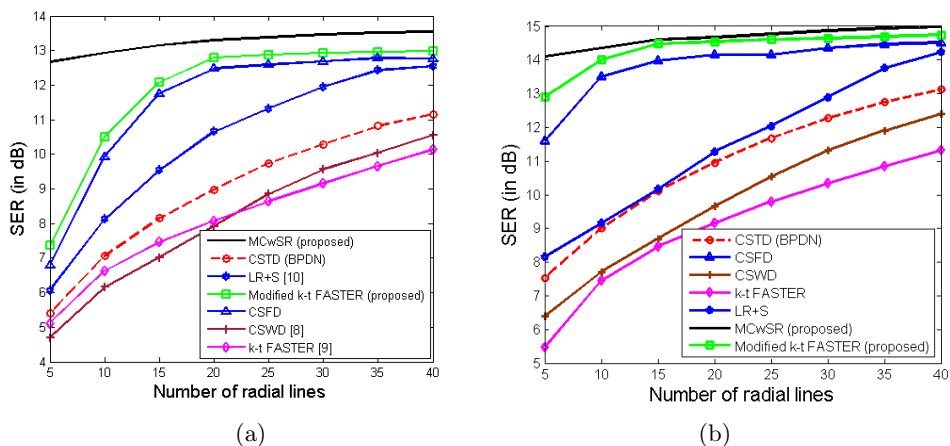


Figure 7: SER vs number of radial lines; (a) Subject 1 Dataset-1, (b) Subject 1 Dataset-2

Group-level reconstruction analysis

Fig.8a and Fig.8b depicts NMSE results averaged over all volumes and over all slices on dataset-1 and 2, respectively. 12 radial lines are used for under-

sampling of the k - t space data. We present results on first five subjects of each dataset. We observe that for dataset-1 MCwSR is consistently giving better results compared to all the methods for all subjects.

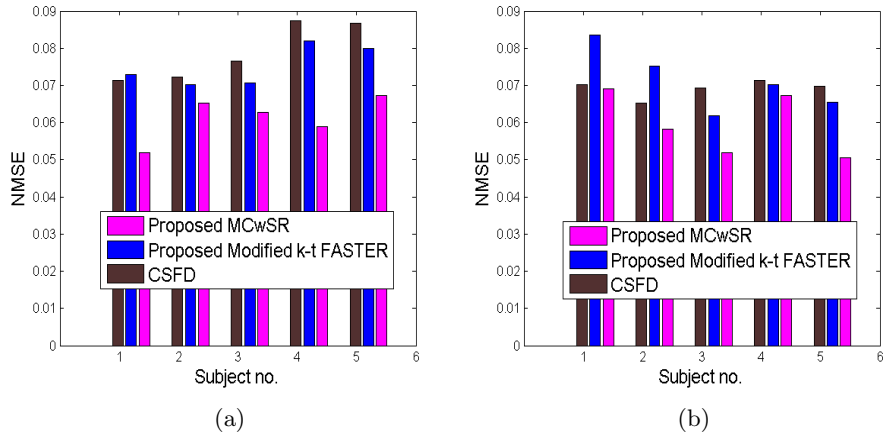


Figure 8: NMSE vs subject number using 12 radial lines:
(a) dataset-1 Middle slice 18, (b) dataset-2 Middle slice 16

Statistical analysis for activation maps

In this section, we explore the quality of voxel activation maps for the fMRI data reconstructed using the above methods. To this end, first pre-processing of fMRI data is done in SPM. In this stage, fMRI data are realigned for removal of motion artifact. Smoothing is also a standard pre-processing step that is generally carried out to improve signal-to-noise ratio (SNR). It is one of the preprocessing step before statistical analysis in fMRI literature. This helps with denoising of data and hence, SNR. This improves sensitivity of the analysis and better activation maps are obtained. Since the proposed reconstruction method inherently denoises the data, we claim that this step is not needed with the proposed MCwSR method. In order to validate this claim, we show time-series profile of some voxels of 18th slice of dataset-1 reconstructed with MCwSR method in Fig.9a. Fig.9b shows time-series profile of some voxels of 16th slice of dataset-2. This figure presents time-series profiles of fully sampled and reconstructed fMRI data (using the proposed MCwSR method). It is observed that the reconstructed time series profile is a denoised version of the fully sampled data validating our claim.

In order to further assess this claim and ensure that we do not loose information related to activation detection, we compute activation maps on fMRI data of dataset-1 reconstructed using different methods. After preprocessing, fMRI data is fitted to four input block conditions as mentioned in [19]. These conditions are false belief story, false belief question, false belief photo story,

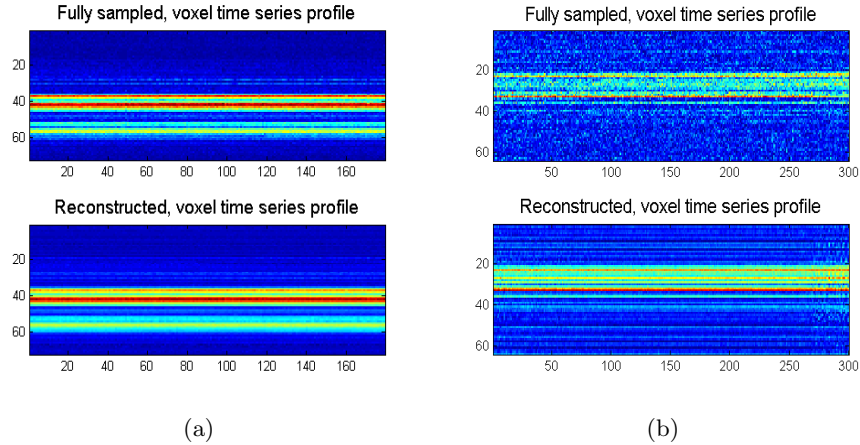


Figure 9: Voxel time series profiles:
(a) dataset-1 Middle slice 18, (b) dataset-2 Middle slice 16

and false belief photo question. We computed task-related activation on reconstructed fMRI data using general linear model (GLM).

GLM is a univariate method used for activation detection on task based fMRI data [32]. In this method, a linear model of applied stimuli is fitted to each voxel time series resulting in a set of voxel specific parameters. These parameters can be used to form statistical parametric maps (SPMs) or contrast maps or activation maps [33]. We generated these activation maps using SPM8² that is a standard fMRI statistical analysis toolbox for MATLAB software. The resulting maps are thresholded using p -value ($p < 0.05$) wherein clusters with atleast 12 voxels are considered active. Maps are generated on reconstructed data and compared with maps of fully sampled ground truth data.

As stated earlier, if the reconstruction method does not incorporate denoising, smoothing is required as a pre-processing step in order to improve SNR and hence, have correct activation detection. Thus, we present activation maps with the original fully sampled (noisy) data without smoothing, original fully sampled data after smoothing (Full Width Half Maximum, FWHM, $6mm$), and with different accelerated (12 radial lines, 6.065 acceleration factor) reconstruction methods without smoothing in Fig.10.

On visually comparing these activation maps, we observe that the activation map with accelerated McwSR method (without smoothing) in Fig.10(i) is similar to that of fully sampled data with smoothing as shown in Fig. 10(b). This result show that proposed MCwSR reconstruction method has an inherent ability to improve SNR and hence, activation maps of reconstructed data is close to fully sampled data with smoothing as shown in Fig.10 (b). This is an added advantage of the proposed MCwSR reconstruction method. Since MCwSR, modified k-t FASTER, and CSFD methods are performing better compared to other, we have

²<http://www.fill.ion.ucl.ac.uk/spm/>

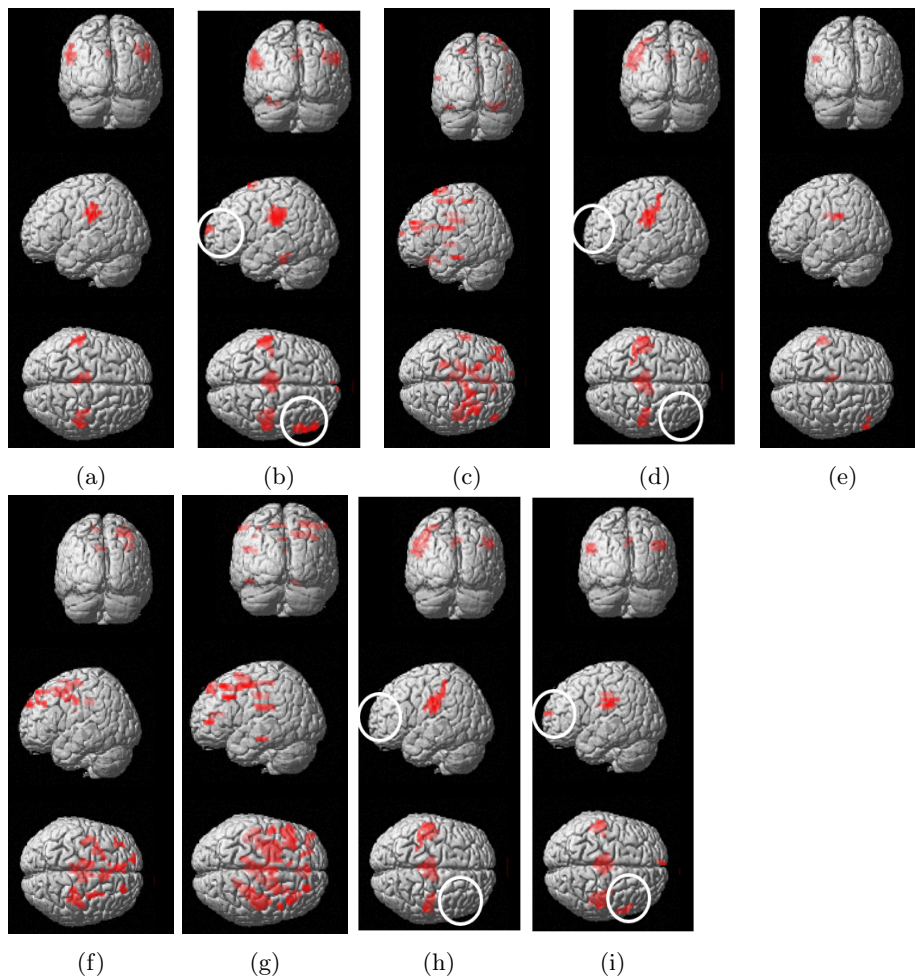


Figure 10: Activation maps in coronal (row-1), sagittal (row-2), and axial (row-3) planes on Dataset-1 using:
(a) Original (noisy) fully-sampled data, (b) Original fully-sampled data with FWHM 6mm smoothing, (c)-(i) on accelerated (12 radial lines based) reconstructed data using (c) k - t FASTER, (d) Proposed Modified k - t FASTER, (e) LR+S, (f) CSTD (BPDN), (g) CSWD, (h) CSFD, (i) Proposed MCwSR

highlighted these results via white circles in Fig. 10d (modified k - t FASTER), Fig. 10h (CSFD), and Fig. 10i (MCwSR). The activation shown in red in the circled area in Fig. 10b seems to be lost in Fig. 10d and Fig. 10h, while it is preserved in Fig. 10i. This again validates our claim that the proposed MCwSR reconstruction method also improves SNR without losing activation. Further, we observe that false positives are detected with CSTD (BPDN), CSWD, k - t FASTER, and LR+S methods that can yield misleading findings on fMRI

data. Thus, this paper also demonstrates a way of validating the reconstruction method on fMRI data.

6. Conclusions

In this paper, we have supported the literature of accelerated fMRI reconstruction by proposing a new fMRI reconstruction method. The proposed method exploits both sparsity and low-rank to improve fMRI reconstruction accuracy and is named as Matrix completion with Sparse Recovery (MCwSR). This method is implemented via Split Bregman algorithm. We compared the performance of the proposed method with some methods including k - t FASTER, LR+S, CSTD or BPDN, CS with wavelet sparsity, CS with Fourier sparsity, and modified k - t FASTER on two real fMRI dataset. Our results show that the proposed MCwSR method yields the most faithful reconstruction both quantitatively and qualitatively. Further, MCwSR method's performance is consistently good at very low sampling ratios.

In addition, this proposed method is able to preserve the voxel activation map of fMRI data that is not observed with any other existing method. Rather, most of the existing methods provide false activation that can yield misleading findings on fMRI data. This establishes the significance of the proposed method. In addition, this paper has provided a mechanism to validate the reconstruction quality of an fMRI reconstruction method via building brain activation maps.

Acknowledgements

The first author would like to thank Visvesvaraya research fellowship, Department of Electronics and Information Tech., Ministry of Comm. and IT, Govt. of India, for providing financial support for this work.

References

- [1] N. K. Logothetis, What we can do and what we cannot do with fMRI, in: Nature, 869–878, 2008.
- [2] J. K. Huttunen, O. Grhn, M. Penttonen, Coupling between simultaneously recorded {BOLD} response and neuronal activity in the rat somatosensory cortex, NeuroImage 39 (2) (2008) 775 – 785.
- [3] P. Jezzard, A. W. Song, Technical Foundations and Pitfalls of Clinical fMRI, NeuroImage 4 (3) (1996) S63 – S75.
- [4] S. Ogawa, T. M. Lee, A. R. Kay, D. W. Tank, Brain magnetic resonance imaging with contrast dependent on blood oxygenation., Proc Natl Acad Sci U S A 87 (24) (1990) 9868–9872.

- [5] D. A. Feinberg, S. Moeller, S. M. Smith, E. Auerbach, S. Ramanna, M. F. Glasser, K. L. Miller, K. Ugurbil, E. Yacoub, Multiplexed Echo Planar Imaging for Sub-Second Whole Brain fMRI and Fast Diffusion Imaging, *PLoS ONE* 5 (12) (2010) e15710.
- [6] W. Lu, T. Li, I. Atkinson, N. Vaswani, Modified-CS-residual for recursive reconstruction of highly undersampled functional MRI sequences, in: 18th IEEE International Conference on Image Processing (ICIP), 2689–2692, 2011.
- [7] S. Yan, L. Nie, C. Wu, Y. Guo, Linear Dynamic Sparse Modelling for functional MR imaging, *Brain Informatics* 1 (1-4) (2014) 11–18.
- [8] D. J. Holland, C. Liu, X. Song, E. L. Mazerolle, M. T. Stevens, A. J. Sederman, L. F. Gladden, R. C. N. D’Arcy, C. V. Bowen, S. D. Beyea, Compressed sensing reconstruction improves sensitivity of variable density spiral fMRI, *Magnetic Resonance in Medicine* 70 (6) (2013) 1634–1643.
- [9] M. Chiew, S. M. Smith, P. J. Koopmans, N. N. Graedel, T. Blumensath, K. L. Miller, k-t FASTER: Acceleration of functional fMRI data acquisition using low rank constraints, *Magnetic Resonance in Medicine* 74 (2) (2015) 353–364.
- [10] V. Singh, A. Tewfik, D. Ress, Under-sampled functional MRI using low-rank plus sparse matrix decomposition, in: IEEE International Conference on Acoustics, Speech and Signal Processing (ICASSP), 897–901, 2015.
- [11] D. Donoho, Compressed sensing, *Information Theory, IEEE Transactions on* 52 (4) (2006) 1289–1306.
- [12] L. R. Frank, R. B. Buxton, E. C. Wong, Estimation of respiration-induced noise fluctuations from undersampled multislice fMRI data, *Magnetic Resonance in Medicine* 45 (4) (2001) 635–644.
- [13] A. K. Nemani, I. C. Atkinson, K. R. Thulborn, Investigating the consistency of brain activation using individual trial analysis of high-resolution fMRI in the human primary visual cortex, *NeuroImage* 47 (4) (2009) 1417 – 1424.
- [14] M. Afonso, J. M. Sanches, Image reconstruction under multiplicative speckle noise using total variation, *Neurocomputing* 150, Part A (2015) 200 – 213, ISSN 0925-2312.
- [15] Y. Shen, J. Li, Z. Zhu, W. Cao, Y. Song, Image reconstruction algorithm from compressed sensing measurements by dictionary learning, *Neurocomputing* 151, Part 3 (2015) 1153 – 1162, ISSN 0925-2312.
- [16] N. Eslahi, A. Aghagolzadeh, S. M. H. Andargoli, Image/video compressive sensing recovery using joint adaptive sparsity measure, *Neurocomputing* (2016) –ISSN 0925-2312.

- [17] X. Gao, F. Jiang, S. Liu, W. Che, X. Fan, D. Zhao, Hierarchical frame based spatiotemporal recovery for video compressive sensing coding, *Neurocomputing* 174, Part A (2016) 404 – 412, ISSN 0925-2312.
- [18] Z.-P. Liang, SPATIOTEMPORAL IMAGING WITH PARTIALLY SEPARABLE FUNCTIONS, in: 4th IEEE International Symposium on Biomedical Imaging: From Nano to Macro (ISBI), 988–991, 2007.
- [19] J. M. Moran, E. Jolly, J. P. Mitchell, Social-Cognitive Deficits in Normal Aging, *The Journal of Neuroscience* 32 (16) (2012) 5553–5561.
- [20] T. Schonberg, C. R. Fox, J. A. Mumford, E. Congdon, C. Trepel, R. A. Poldrack, Decreasing ventromedial prefrontal cortex activity during sequential risk-taking: An fMRI investigation of the Balloon Analogue Risk Task, *Frontiers in Neuroscience* 6 (80).
- [21] J.-F. Cai, S. Osher, Z. Shen, Split Bregman methods and frame based image restoration, *Multiscale modeling & simulation* 8 (2) (2009) 337–369.
- [22] T. Goldstein, S. Osher, The split Bregman method for L1-regularized problems, *SIAM Journal on Imaging Sciences* 2 (2) (2009) 323–343.
- [23] S. Boyd, N. Parikh, E. Chu, B. Peleato, J. Eckstein, Distributed Optimization and Statistical Learning via the Alternating Direction Method of Multipliers, *Found. Trends Mach. Learn.* 3 (1) (2011) 1–122.
- [24] J.-F. Cai, E. J. Candès, Z. Shen, A Singular Value Thresholding Algorithm for Matrix Completion, *SIAM J. on Optimization* 20 (4) (2010) 1956–1982.
- [25] S. Ma, D. Goldfarb, L. Chen, Fixed point and Bregman iterative methods for matrix rank minimization, *Mathematical Programming* 128 (1-2) (2011) 321–353.
- [26] I. W. Selesnick, *Sparse Signal Restoration*, 2010.
- [27] H. Zhu, Y. Xiao, S.-Y. Wu, Large sparse signal recovery by conjugate gradient algorithm based on smoothing technique, *Computers & Mathematics with Applications* 66 (1) (2013) 24 – 32.
- [28] S. Zhang, K. T. Block, J. Frahm, Magnetic resonance imaging in real time: Advances using radial FLASH, *Journal of Magnetic Resonance Imaging* 31 (1) (2010) 101–109.
- [29] S. S. Chen, D. L. Donoho, M. A. Saunders, Atomic Decomposition by Basis Pursuit, *SIAM Rev.* 43 (1) (2001) 129–159.
- [30] F. Lin, T.; Herrmann, Compressed extrapolation, *Geophysics* 72 (2007) 77–93.
- [31] P. C. Hansen, Analysis of Discrete Ill-posed Problems by Means of the L-curve, *SIAM Rev.* 34 (4) (1992) 561–580.

- [32] M. A. Lindquist, The Statistical Analysis of fMRI Data, *Statist. Sci.* 23 (4) (2008) 439–464.
- [33] K. Friston, J. Ashburner, S. Kiebel, T. Nichols, W. E. Penny, *Statistical Parametric Mapping: The analysis of functional brain images*, Academic Press, 2006.